ECS Transactions, 35 (4) 191-204 (2011)
10.1149/1.3572283 ©The Electrochemical Society

Plasma-Assisted Atomic Layer Deposition of Low Temperature SiO_2

G. Dingemans, C. A. A. van Helvoirt, M. C. M. van de Sanden, and W. M. M. Kessels

Department of Applied Physics, Eindhoven University of Technology, P.O. Box 513, 5600 MB Eindhoven, The Netherlands,

Atomic layer deposition (ALD) was used to deposit SiO_2 films in the temperature range of 50-400 ^oC. $H_2Si[N(C_2H_5)_2]_2$ and an O_2 plasma were used as Si precursor and oxidant, respectively. The growth process was characterized in detail, using various in situ diagnostics. Ultrashort precursor doses (~50 ms) were found to be sufficient to reach self-limiting ALD growth with a growth-per-cycle of ~1 Å. The films exhibited a refractive index of 1.46 ± 0.02, a mass density of 2.0 ± 0.1 g/cm^3, and an O/Si ratio of 2.1 ± 0.1, virtually independent of the substrate temperature. The results therefore demonstrate an efficient ALD process for the conformal and uniform deposition of SiO_2 at low substrate temperatures. Also the surface chemistry during the plasma ALD process and surface passivation performance of the ALD SiO_2 films on crystalline silicon surfaces are briefly addressed.

Introduction

The key importance of silicon dioxide (SiO_2) for applications in silicon-based microelectronics needs no introduction. Also in silicon photovoltaics SiO_2 is a key material, as it has for long been the state-of-the-art passivation material leading to a substantial reduction of the surface recombination losses enabling high solar cell efficiencies [1-4]. High quality SiO_2 is obtained by thermal oxidation of the Si surface at temperatures > 800°C. Alternative methods for the synthesis of SiO_2 have been developed to avoid such high temperatures and long processing times. They may also enable single side deposition and a high level of control of the material properties and film thickness. These alternative methods include (wet) chemical oxidation, (plasma-enhanced) chemical vapor deposition, sputtering and electron beam evaporation.

Atomic layer deposition (ALD) is an alternative CVD-like method that recently gained a lot of attention. ALD allows for precise thickness control, optimal large-area uniformity, and the conformal coating of demanding substrate topologies [5,6]. In a first report, ALD SiO_2 was synthesized employing $SiCl_4$ and H_2O [7,8] which required relatively high substrate temperatures (> 300 ^oC) and long precursor exposures. In recent years, various alternative Si precursors have been tested in combination with O_3 or H_2O as the oxidants. These processes include the use of pyridine (C_5H_5N) [9] and Al as catalysts [10,11]. The approach employing Al was referred to as rapid ALD as it resulted in deposition rates above the “theoretical” maximum of one monolayer per ALD cycle. In addition, more recently a thermal ALD process for low-temperature SiO_2 was reported which was free of catalysts or corrosive by-products [12]. In this respect, the use of precursors with amino ligands has also shown promising results, in particular when combined with H_2O_2, O_3, or O_2 plasma as the oxidant [13-16]. SiO_2 films grown with ALD have been reported to exhibit low carbon content, and a high electrical breakdown

Downloaded 01 May 2011 to 131.155.217.116. Redistribution subject to ECS license or copyright; see http://www.ecsdl.org/terms_use.jsp

field [9,14]. Nevertheless, to improve properties such as the chemical etch rate or the interface defect density, annealing at a temperature of 1000°C was shown to be beneficial [12].

In this contribution an efficient plasma-assisted ALD process is demonstrated for the low-temperature synthesis of SiO_2 using $H_2Si[N(C_2H_5)_2]_2$ as the Si precursor (Figure 1a). This precursor is commercially supplied by Air Liquide under the product name SAM.24 [17,18]. Data are presented for the ALD process within the temperature range of 50-400 °C and the results are compared to the Al_2O_3 ALD processes from $Al(CH_3)_3$ and H_2O/O_2 plasma. These Al_2O_3 processes have been widely studied and are considered rather typical and "ideal" ALD processes [19]. Moreover for ALD Al_2O_3 films excellent surface passivation properties for silicon of arbitrary doping types and different doping levels have been reported [20,21]. In addition, the surface chemistry during the plasma ALD process of SiO_2 is discussed and also the first results on the surface passivation performance of the ALD SiO_2 films on crystalline silicon surfaces are briefly addressed.

Experimental

The SiO_2 films were deposited in the Oxford Instruments OpAL reactor. This is an open-load system, suited for both plasma and thermal ALD and operating at typical pressures of 150 mTorr. A remote O_2 plasma was used during the oxidation step in the ALD cycle. SAM.24 (Air Liquide) was used as the Si precursor (Figure 1a) [17,18]. This is a liquid (melting point < -10 °C) which exhibits a high vapor pressure, i.e. ~100 Torr at 100 °C (Figure 1b). The SAM.24 was held in a stainless steel bubbler heated to 50 °C and the precursor was introduced into the reactor by ultrashort doses (10-120 ms) using fast ALD valves. A flow of Ar as well as the O_2 flow were continuously on during the process. The latter was feasible as no evidence was found for reactions between the Si precursor and O_2 under the experimental conditions used. The substrate temperature during deposition, T_{dep}, was varied between 50 and 400 °C. The reactor wall temperature was 180 °C unless the substrate temperature was lower. Under these conditions the wall and substrate temperature were equal. To allow for direct comparison, Al_2O_3 was synthesized in the same reactor using $Al(CH_3)_3$ as the metal precursor and H_2O or O_2 plasma as the oxidant [19-21]. All films were deposited on Si (100) wafers which received a short treatment in diluted HF (~1% in DI-H_2O) to remove the native oxide prior to loading in the ALD reactor.

In situ spectroscopic ellipsometry (SE) measurements were used for optimizing the ALD process. The growth-per-cycle, GPC, and refractive index were determined by using a Cauchy optical model to fit the ellipsometry data. Rutherford backscattering spectroscopy (RBS) and elastic recoil detection (ERD) employing ~2 MeV He^{2+}-ions from the singletron at the Eindhoven University of Technology and transmission Fourier transform infrared absorption (FTIR) measurements were used to analyze the film composition. The surface morphology was investigated by atomic force microscopy (AFM) measurements in semi-contact mode whereas high-resolution transmission electron microscopy (TEM) was used to study the samples in cross-section. The deposition process itself was studied in real time by quadrupole mass spectroscopy (QMS) probing the gas in the exhaust line and by optical emission spectroscopy (OES) through a view port located on top of the ALD reactor.

Downloaded 01 May 2011 to 131.155.217.116. Redistribution subject to ECS license or copyright; see http://www.ecsdl.org/terms_use.jsp

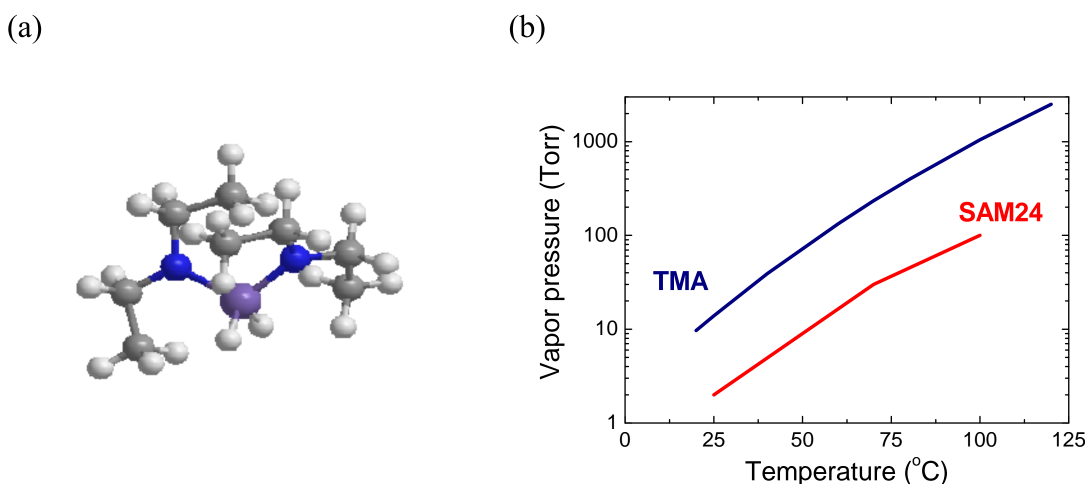

Figure 1. (a) The precursor $H_2Si[N(C_2H_5)_2]_2$ (SAM.24, Air Liquide) used for ALD of SiO_2 and (b) the vapor pressure of the precursor as a function of the temperature. The vapor pressure is compared to the one of $Al(CH_3)_3$ (trimethylaluminum, TMA). This precursor is commonly used for ALD of Al_2O_3.

The passivation performance of the ALD SiO_2 films was evaluated from the effective lifetime τ_{eff} of the minority carriers in double-side coated floatzone *n*-type Si wafers (~3.5 Ω cm). τ_{eff} was determined with photoconductance decay in the transient mode and quasi-steady-state-mode (for $\tau_{eff} < 100$ μs) using a Sinton lifetime tester (WCT 100). The upper level for the surface recombination velocity $S_{eff,max}$ was extracted at an injection level of 5×10^{14} cm^{-3} by the expression

$$S_{eff,max} = \frac{W}{2\cdot\tau_{eff}}, \quad (1)$$

with *W* the thickness of the silicon wafer (~280 μm). In the derivation of this expression it is assumed that all recombination takes place at the surface.

Results and discussion

ALD Growth Process

The ALD process was monitored by in situ spectroscopic ellipsometry by taking data points after a certain number of cycles. Typical thickness data plotted as a function of number of ALD cycles are shown in Figure 2 for the substrate temperatures of 50 °C and 250 °C. For 250 °C the SiO_2 thickness increased linearly with the number of cycles (the data for 50 °C will be discussed below). The slope of the curve yields the growth-per-cycle (GPC) and for a substrate temperature of 250 °C a GPC value of 1.1 Å/cycle is obtained. This GPC value is very comparable to the plasma-assisted ALD process of Al_2O_3 [19,20]. Moreover, no indications for a significant growth delay on the H-terminated Si(100) substrates were observed for the SiO_2 ALD process. This is also similar to what has been observed for plasma ALD of Al_2O_3 [19].

Downloaded 01 May 2011 to 131.155.217.116. Redistribution subject to ECS license or copyright; see http://www.ecsdl.org/terms_use.jsp

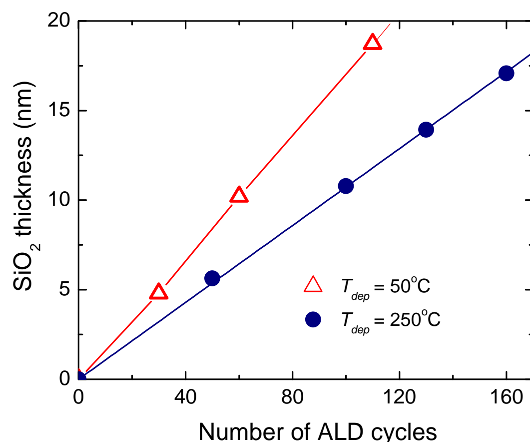

Figure 2. SiO_2 film thickness as a function of the number of ALD cycles at substrate temperatures of 50 °C and 250 °C. The film thickness was measured by in situ spectroscopic ellipsometry.

Figure 3 shows the effect of the duration of the successive steps in the ALD recipe, i.e., the precursor dosing, precursor purge step, plasma exposure, and plasma exposure purge step (Figure 1a-1d). In the corresponding experiments one process parameter in the ALD recipe was varied whereas the duration of the other steps was taken sufficiently long to guarantee saturated ALD conditions for the non-varied process parameters. The substrate temperature was set to 250 °C. The growth process of SiO_2 is compared to plasma-assisted ALD of Al_2O_3 at 250 °C (Figure 1e-1h). From the figure it is evident that ultrashort precursor dosing times (~50 ms) were already sufficient to reach a self-limiting growth with a GPC of ~1.1 Å. These short dosing times were only slightly higher compared to those used for the $Al(CH_3)_3$ precursor for ALD of Al_2O_3. The fact that short dosing times are sufficient is in agreement with the expectations based on the relatively high vapor pressure of the SAM.24 precursor. Many other processes from different precursors require much longer dosing times, for instance ALD of TiO_2 and Ta_2O_5 require dosing times > 1s in a similar remote plasma and thermal ALD reactor [22,23]. The duration of the purge step after precursor dosing was required to be > 2 s. For shorter purge times, residual precursor remaining in the reactor volume can react in the plasma, causing parasitic (PE)CVD-like growth and a higher GPC value. Regarding the O_2 plasma step, a plasma exposure time > 1 s was found to be sufficient to reach a saturated GPC, indicating the rapid removal of the precursor ligands. This plasma exposure time is slightly shorter than for plasma ALD of Al_2O_3 which requires plasma times of ~2 s to reach saturated growth. However with in situ spectroscopic ellipsometry only the center of the Si wafer is probed and therefore, to ensure saturation over full wafer surface, a plasma exposure time of 4 s was employed in all subsequent experiments. Interestingly, the purge after the plasma step had a significant impact on the GPC. This is in contrast to the ALD process for Al_2O_3, where the purge step after O_2 plasma exposure was found to have little influence on the GPC and could be reduced well below 0.5 s. We attribute the higher GPC for shorter purges (< 2 s) to reactions between residual H_2O, formed during the plasma process, with the Si precursor injected in the subsequent step. Although it is known that the $H_2Si[N(C_2H_5)_2]_2$ precursor reacts with H_2O, it is relevant to mention here that we were unable to develop a thermal ALD process for SiO_2 using

Downloaded 01 May 2011 to 131.155.217.116. Redistribution subject to ECS license or copyright; see http://www.ecsdl.org/terms_use.jsp

SAM.24 as precursor and H_2O as the oxidant. No film growth was observed. Instead, even with the shortest possible H_2O doses applied, powder formation occurred in the reactor as was noticeable by the naked eye.

Figure 3 also shows the refractive index of the films corresponding to the experiments to verify saturation of the SiO_2 ALD process. At a photon energy of 2 eV a refractive index of 1.46±0.02 was obtained for the SiO_2 films under the saturated ALD conditions. The refractive index was observed to drop for very short dose and purge times, most prominently for a too short plasma exposure time. This can most probably be attributed to a reduced SiO_2 density under these conditions.

The thickness uniformity of the SiO_2 films deposited by plasma-assisted ALD at 250 ^{o}C was evaluated by mapping the thickness by spectroscopic ellipsometry. For a 8 inch (200 mm) wafer the nonuniformity, defined by the difference between the maximum and minimum thicknesses divided by the twice the average thickness of all data points measured [19], was < 3.5%. The thickness nonuniformity achieved on 4 inch (100 mm) wafers was ~1%.

Material Properties and Substrate Temperature Dependence

Figure 4 shows the effect of the substrate temperature between 50 and 400 ^{o}C on the ALD growth process of SiO_2. The length of the purge steps in the lower temperature regime was extended (up to 10 s at 50 ^{o}C) as it is more difficult to remove H_2O at lower temperatures which could impact the saturation behavior of the process. The GPC was observed to decrease with increasing deposition temperature from ~1.7 Å/cycle at 50 ^{o}C to 0.8 Å at 400 ^{o}C. The refractive index was fairly constant between 100 and 300 ^{o}C. Below 100 ^{o}C and above 300 ^{o}C the refractive index was somewhat lower and it can therefore not be excluded that some non-ideal ALD behavior takes place at the lowest and highest temperatures investigated. At the low substrate temperature of 50 ^{o}C, additional CVD reactions may contribute to the higher GPC. This might also explain the slightly non-linear trend between the film thickness and number of cycles observed at this deposition temperature as shown in Figure 2. The slightly increasing GPC with number of ALD cycles points to the accumulation of some residual H_2O in the reactor with which the precursor can react, despite the long purging times (10 s) after the plasma step. For temperatures reaching 400 ^{o}C thermal stability issues of the precursor and its ligands can start to play a role.

Table 1 shows RBS and ERD data obtained at substrate temperatures of 100, 200 and 300 ^{o}C. The table shows that the number of Si atoms deposited per cycle decreases with increasing substrate temperature. This clearly demonstrates that the decrease of the GPC with increasing substrate temperature can be attributed to reduced precursor adsorption per cycle at higher temperatures. Similar results were obtained for Al_2O_3 synthesized by plasma-assisted ALD [19,20,23]. As shown in Figure 4c, the GPC for this process was also found to decrease significantly when going from 25 to 400 ^{o}C. This could be attributed almost fully to the decrease in the number of Al atoms deposited per cycle. Film densification, decreasing the thickness per "monolayer" of Al_2O_3 deposited, was found to play a minor role and only for temperatures well below 100 ^{o}C. For Al_2O_3, the decrease in GPC with increasing temperature could be attributed to a loss of –OH surface groups with increasing temperature due to thermally activated dehydroxylation reactions [6,24,25]. Thermal ALD of Al_2O_3 (Figure 4c) exhibited a different trend for substrate temperatures < 200°C. For these temperatures the ALD process was not ruled by the density of –OH surface groups but rather by the reduced oxidation efficiency of H_2O at the lower substrate temperatures [19,24].

Downloaded 01 May 2011 to 131.155.217.116. Redistribution subject to ECS license or copyright; see http://www.ecsdl.org/terms_use.jsp

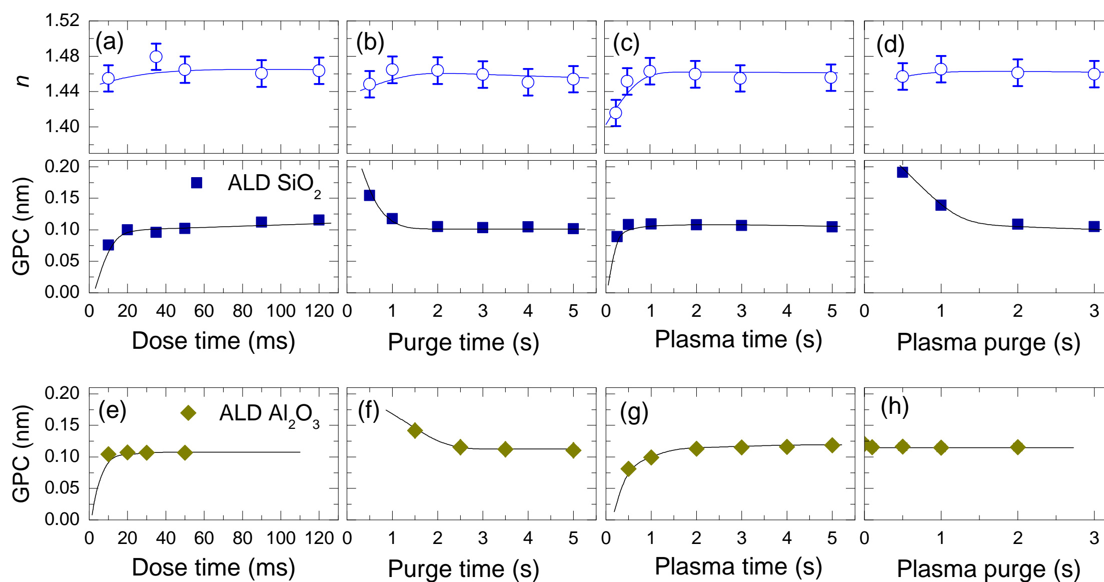

Figure 3. (a)-(d) Saturation curves for the growth-per-cycle GPC and refractive index *n* of the SiO_2 films as measured by in situ spectroscopic ellipsometry as a function of the 4 process parameters in the ALD recipe. (e)-(h) Saturation curves for the GPC of Al_2O_3 films. The substrate temperature was 250 ^{o}C for both the SiO_2 and Al_2O_3 process.

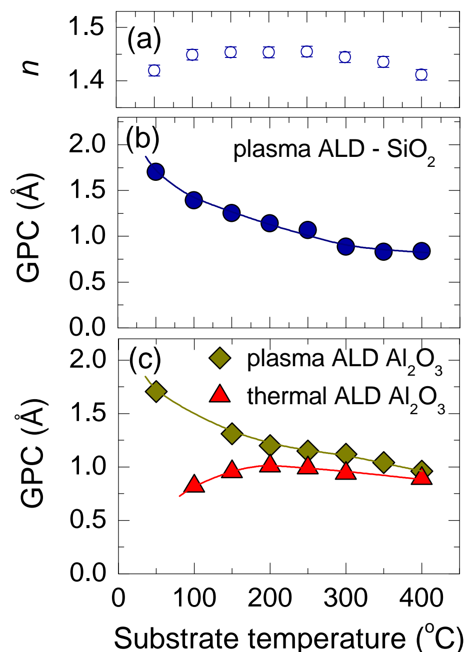

Figure 4. Influence of the substrate temperature during deposition on (a) the refractive index *n* and (b) the growth-per-cycle GPC of SiO_2 as determined with in situ spectroscopic ellipsometry. In (c) the GPC is given for plasma and thermal ALD of Al_2O_3.

Downloaded 01 May 2011 to 131.155.217.116. Redistribution subject to ECS license or copyright; see http://www.ecsdl.org/terms_use.jsp

Table 1. Data on ALD SiO_2 as determined from the RBS and ERD measurements. In the calculation of the mass density the film thickness as obtained by SE was used. The thickness of the films was in the range of 35 – 45 nm.

Substrate temperature (^{o}C)	Si atoms per cycle (10^{14} cm^{-2})	[Si] (at.%)	[O] (at.%)	[H] (at.%)	O/Si ratio	mass density (g/cm^3)
100	2.8 ± 0.1	29.1 ± 0.8	61.3 ± 1.5	9.6 ± 0.9	2.1 ± 0.1	2.0 ± 0.1
200	2.3 ± 0.1	29.9 ± 0.8	62.9 ± 1.5	7.1 ± 0.7	2.1 ± 0.1	2.0 ± 0.1
300	1.9 ± 0.1	29.6 ± 0.8	62.3 ± 1.5	8.1 ± 0.8	2.1 ± 0.1	2.1 ± 0.1

The fact that good SiO_2 material properties were obtained between 100 and 300 ^{o}C can be concluded from Table 1. The Si and O content correspond with an O/Si ratio of 2.1 ± 0.1 and the hydrogen content of the films is 7 – 10 at.% depending on the substrate temperature. The carbon and nitrogen content of the films was below the detection limit of ~5 at.%. Apart from the hydrogen content, the materials properties were found virtually independent of the substrate temperature in the range of 100 – 300 ^{o}C. This also holds for the mass density which was found to be 2.0 ± 0.1 g/cm^3. The film quality was therefore fairly constant for the plasma ALD SiO_2 process. For the plasma-assisted ALD process of Al_2O_3 the variation in film properties also remained within a narrow range, although the variation with temperature was slightly more pronounced compared to SiO_2 prepared by plasma ALD. For Al_2O_3 deposited at temperatures between 100 and 400 ^{o}C, the O/Al ratio varied between 1.5 and 1.7, and the mass density between 2.9 and 3.2 g/cm^3 [19,20]. The hydrogen content of the Al_2O_3 was in the range 1-8 at.% decreasing with increasing substrate temperature whereas carbon could not be detected above the detection limit of the RBS measurements. For temperatures below 100 ^{o}C, the Al_2O_3 became more O-rich, less dense, and contained significantly more hydrogen [19,20].

Fourier transform infrared absorption spectroscopy was used to compare the ALD SiO_2 films with thermally-grown SiO_2. Figure 5 shows the FTIR spectra revealing a shift of the Si-O-Si stretching and Si-O-Si rocking modes toward lower wavenumbers for the ALD SiO_2 film. This is in agreement with the slightly non-stoichiometric nature (O/Si ratio = 2.1 ± 0.1) of the films and the fact that the mass density of ALD SiO_2 is slightly lower compared to typical values for wet thermally grown SiO_2 films (~2.2 g/cm^3). The FTIR data also confirm the presence of hydrogen in the ALD SiO_2 films by the observation of SiO-H bending (~920 cm^{-1}) and SiO-H stretching (2500-3600 cm^{-1}) signatures in the spectrum.

The surface morphology of the SiO_2 films was studied by AFM in semi-contact mode. Films deposited at a substrate temperature of 100 ^{o}C (film thickness is 51 nm) and 200 ^{o}C (film thickness is 48 nm) were compared. The AFM scan of the SiO_2 film deposited at 200 ^{o}C is shown in Figure 6 and reveals a root-mean-square surface roughness of 1.6 Å. The film deposited at 100 ^{o}C, exhibited only a slightly higher roughness of 1.9 Å. These values were similar to those obtained for uncoated polished Si wafers and this demonstrates that the films show negligible roughness development on the Si(100) substrate. The latter can also be appreciated from the high-resolution TEM image displayed in Fig. 7. From the AFM data it also follows that the aforementioned (PE)CVD growth component at lower substrate temperatures caused by residual H_2O is not pronounced yet at 100 ^{o}C.

Downloaded 01 May 2011 to 131.155.217.116. Redistribution subject to ECS license or copyright; see http://www.ecsdl.org/terms_use.jsp

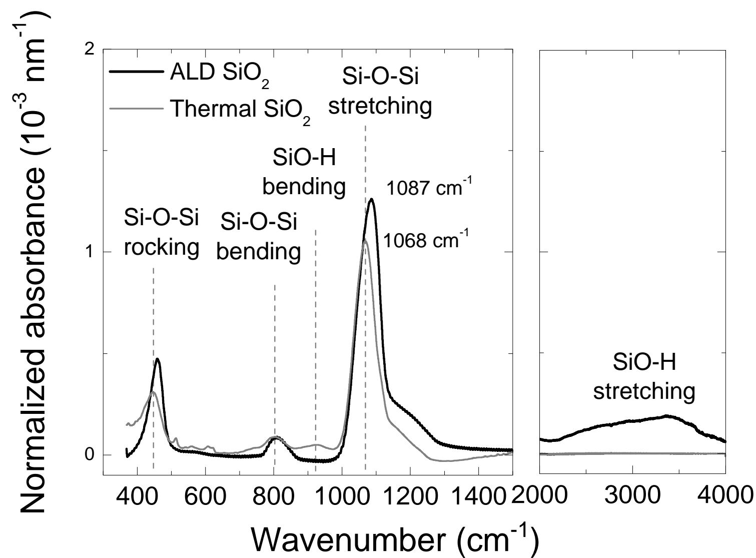

Figure 5. FTIR spectra of ALD SiO_2 prepared at 200 °C (48 nm film thickness) and thermal SiO_2 grown by wet oxidation at ~900°C (295 nm film thickness). The most prominent absorption peaks have been assigned (see Ref. 24 and references therein). The absorbance is normalized by the film thickness. A Si wafer without SiO_2 served as a reference to obtain the absorption spectra.

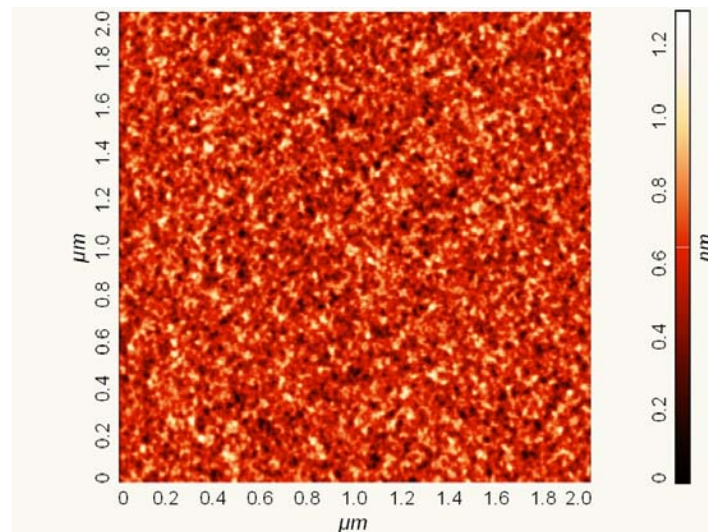

Figure 6. AFM scan of an ALD SiO_2 film deposited at a substrate temperature of 200 °C. The thickness of the film was 48 nm. The scan size was 2 μm × 2 μm.

Downloaded 01 May 2011 to 131.155.217.116. Redistribution subject to ECS license or copyright; see http://www.ecsdl.org/terms_use.jsp

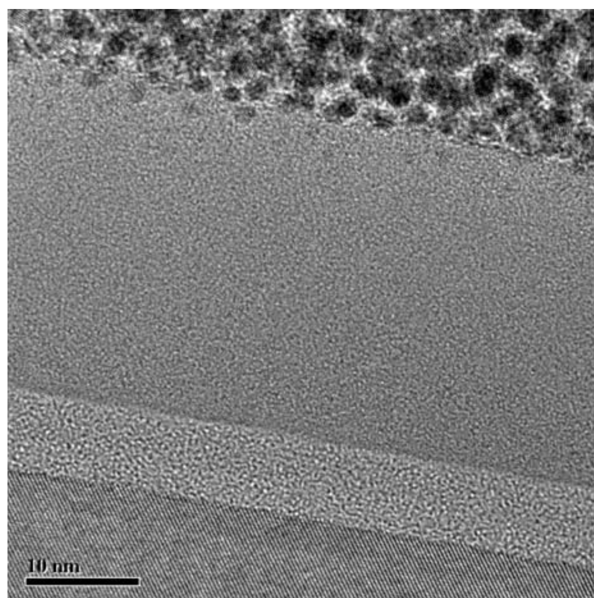

Figure 7. High-resolution TEM image of an ALD SiO_2 film of 7.0 ± 0.3 nm thickness deposited on a H-terminated Si(100) wafer. The SiO_2 was encapsulated by an Al_2O_3 film deposited by plasma-assisted ALD to prepare the sample for TEM analysis.

Surface Chemistry

From the data presented and on the basis of literature reports, also a few comments can be made about the surface chemistry. The GPC decreases monotonically with the substrate temperature which is very similar to the case of Al_2O_3 synthesized by plasma-assisted ALD. It was experimentally verified that the surface chemistry during plasma ALD Al_2O_3 was ruled by –OH groups, with the number density of these –OH groups decreasing with temperature [24,25]. It can therefore be concluded that also the plasma-assisted ALD SiO_2 process is governed by the –OH groups with the decrease of the GPC in Figure 4b ruled by thermally activated dehydroxylation reactions. Moreover, the presence of –OH groups was demonstrated by the FTIR spectrum of the ALD SiO_2 film showing a clear signature of SiO-H bonds incorporated in the film (Figure 5). During the precursor step, it is therefore most likely that the $–N(C_2H_5)_2$ ligands of the precursor react with the surface –OH groups producing volatile $HN(C_2H_5)_2$. A reaction involving the breaking of the Si-H bond in the precursor is very unlikely [16]. We propose therefore similar surface chemical reactions during the first ALD half cycle as reported by Burton *et al*. [16] for the $SiH(N(CH_3)_2)_3$ precursor which is comparable to the present precursor:

$$\text{Si-OH}^* + H_2Si[N(C_2H_5)_2]_2 \rightarrow \text{SiO-SiH}_2[N(C_2H_5)_2]_{2-x}{}^* + x\, HN(C_2H_5)_2,$$

where surface species are indicated by *. In this precursor adsorption reaction, only one (x = 1) or both (x = 2) of the $–N(C_2H_5)_2$ ligands may react. In the second half cycle, the surface reactions will be dominated by O radical species delivered by the plasma [27]. From similar cases studied previously (e.g., Al_2O_3 from $Al(CH_3)_3$ and O_2 plasma [27] and

Downloaded 01 May 2011 to 131.155.217.116. Redistribution subject to ECS license or copyright; see http://www.ecsdl.org/terms_use.jsp

Ta_2O_5 from $Ta[N(CH_3)_2]_5$ and O_2 plasma [22]) it can be hypothesized that combustion-like reactions dominate:

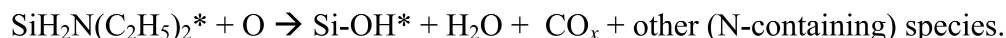

$$SiH_2N(C_2H_5)_2^* + O \rightarrow Si\text{-}OH^* + H_2O + CO_x + \text{other (N-containing) species.}$$

In the latter expression the species are not balanced as it is unclear what reaction products are actually created. In the second half cycle also N-containing species need to be produced for the case that not all precursor molecules react with the –OH covered surface through the release of both $–N(C_2H_5)_2$ ligands, i.e. when $x \neq 2$ for all precursor molecules adsorbing.

Evidence for the fact that $x \neq 2$ for all precursor molecules was obtained from preliminary quadrupole mass spectrometry (QMS) measurements. Figure 8 shows time-dependent mass spectrometry data for a number of selected mass-over-charge *m/z* ratios. The enhanced signals at $m/z = 72$ ($N[C_2H_5]_2^+$) and $m/z = 73$ ($HN[C_2H_5]_2^+$) during the first half cycle are consistent with the removal of the precursor ligands during precursor adsorption. However, it should be noted that these signals can also originate from the cracking of the precursor molecule in the mass spectrometer. Slightly enhanced signals at these *m/z* values were also observed during the second half cycle whereas the signals were absent during steps in which the plasma was ignited without preceding precursor dosing. This suggests that after the first half cycle indeed a fraction of the $-N(C_2H_5)_2$ ligands remain intact on the surface [16]. The latter can also be concluded from the other species observed during the second half cycle. During this plasma step, the prominent *m/z* ratios that were detected included $m/z = 2$ (H_2^+), $m/z = 18$ (H_2O^+), $m/z = 28$ (CO^+) and $m/z = 44$ (CO_2^+). Figure 8 shows the signals at $m/z = 18$ and $m/z = 44$. The fact that combustion products such as CO_2 are observed during the plasma step clearly indicates that some $-N(C_2H_5)_2$ ligands remain on the surface after precursor adsorption.

The interpretation of mass spectrometry for plasma-assisted ALD processes is more complicated than for thermal ALD as the species released from the surface can react in the plasma leading to the creation of new species. The preliminary mass spectrometry data as shown in Figure 8 should therefore be interpreted with care [27]. The plasma however also allows investigation of the optical emission spectrum during the plasma step [28]. Figure 9 shows two optical emission spectra, one for a plasma step during ALD (recorded immmediately after plasma ignition) and one for a regular O_2 plasma without preceding precursor dosing step. The presence of OH and H emission (i.e., H_α, H_β, H_γ of the Balmer series) is clearly observed for the plasma step during ALD. These excited fragments are formed in the plasma by (electron-induced) dissociation of volatile species (likely mostly from H_2O) originating from the reactor surfaces and substrate. The inset shows the transient H_α emission during the plasma step in the ALD cycle. The increase and subsequent decrease of the signal suggests that the reaction products are formed within the first second after plasma ignition. This interpretation is consistent with the fast saturation behavior as displayed in Figure 3c. The H_α emission disappears within 3-4 s after plasma ignition which is similar to the residence time of the particles in our reactor at the operating pressure used (~150 mTorr). This indicates that the surface reactions take place almost instantly after plasma ignition. Interesting is also that no signal due to CN emission is observed during the plasma step. This emission was prominently present in the emission spectra during plasma ALD from Ta_2O_5 from $Ta[N(CH_3)_2]_5$ and O_2 plasma [22].

Downloaded 01 May 2011 to 131.155.217.116. Redistribution subject to ECS license or copyright; see http://www.ecsdl.org/terms_use.jsp

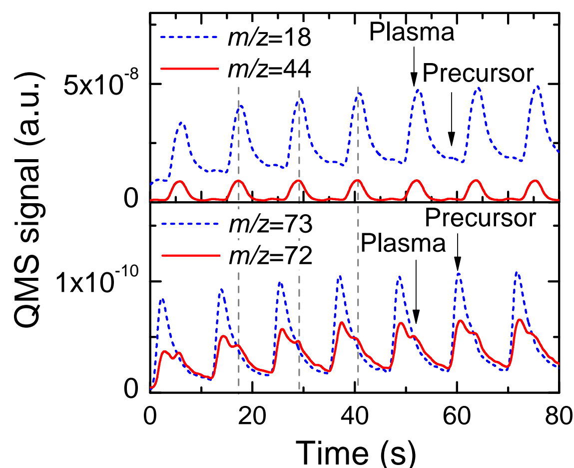

Figure 8. Data from quadrupole mass spectrometry (QMS) for selected mass-over-charge ratios, i.e., m/z = 18 (H_2O^+), 44 (CO_2^+), 72 ($HN[C_2H_5]_2^+$), and 73 ($HN[C_2H_5]_2^+$). During the measurements the substrate temperature was 250 ^oC and the wall temperature was 180 ^oC.

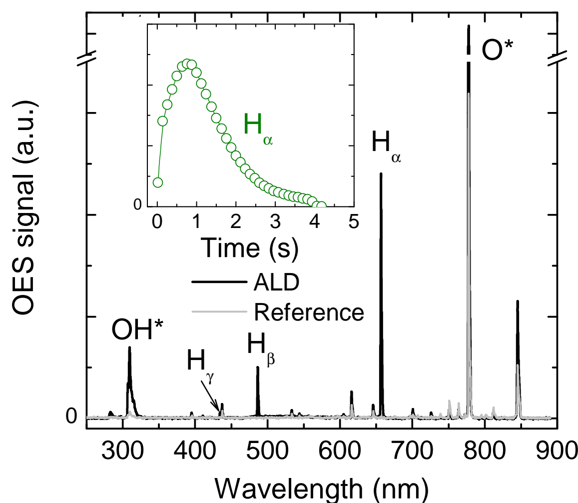

Figure 9. Optical emission spectra (OES) for the plasma step during plasma-assisted ALD and for a regular plasma step without preceding precursor dosing. The latter served as a reference. The most prominent emission lines have been assigned. The inset shows the transient signal due to H_α emission after the ignition of the plasma at 0 s.

Silicon Surface Passivation

Finally, preliminary data on the passivation performance of the ALD SiO_2 films are discussed. As described in the experimental section the passivation properties were evaluated by measuring the effective lifetime τ_{eff} of the minority carriers in floatzone *n*-

Downloaded 01 May 2011 to 131.155.217.116. Redistribution subject to ECS license or copyright; see http://www.ecsdl.org/terms_use.jsp

type Si wafers (~3.5 Ω cm) which were deposited by SiO_2 films of 45 nm thickness at both sides after a treatment of the wafer in diluted HF (~1% in DI-H_2O). The substrate temperature was 200 °C. The films afforded no significant surface passivation in the as-deposited state as indicated by a very low effective lifetime of τ_{eff} = ~4 μs. Similar results were reported for as-deposited plasma ALD Al_2O_3 films [20,29]. These Al_2O_3 films were shown to exhibit a very high defect density at mid gap (~10^{13} eV^{-1} cm^{-2}) related to the VUV radiation present in the plasma [30]. Annealing the ALD SiO_2 films in forming gas (10% H_2 in N_2) at 400 °C for 10 min. led to improved surface passivation with τ_{eff} = 450 μs at an injection level of 5×10^{14} cm^{-3}, which corresponds to $S_{eff,max}$ of 31 cm/s. This value is comparable to the $S_{eff,max}$ of 54 cm/s reached on floatzone *n*-type Si wafers (~1.3 Ω cm) by PECVD SiO_2 films after a 15 min. forming gas anneal at 600 °C [26]. The latter is among the best reported values for films prepared by CVD-like methods. The value of $S_{eff,max}$ is however much higher than the surface recombination velocity achieved by Al_2O_3 films prepared by plasma ALD and thermal ALD after annealing at 400 °C for 10 min. in N_2 [21]. For the same wafers this leads to $S_{eff,max}$ values as low as 0.8 cm/s and 2 cm/s for plasma and thermal ALD, respectively. Moreover, the surface passivation of the ALD SiO_2 films was not stable over time and gradually deteriorated. Issues with the long term stability of the passivation by SiO_2 have been reported before for chemical oxides [31]. Nevertheless, the ALD SiO_2 films are of significant interest for surface passivation of silicon surfaces, for example in combination with Al_2O_3 films as has recently also been demonstrated for PECVD SiO_x [32].

Conclusions

A plasma-assisted ALD process for SiO_2 from the SAM.24 precursor ($H_2Si[N(C_2H_5)_2]_2$) and an O_2 plasma as oxidant has been developed for substrate temperatures between 50 and 400 °C. It is demonstrated that this process is suited for low-temperature synthesis of high-quality SiO_2 by ALD with the SiO_2 properties being relatively insensitive to the substrate temperature for the temperature range of 100 – 300 °C. The process is also relatively fast as it combines a high growth-per-cycle (0.8 – 1.7 Å/cycle) with relatively short dosing and purge times. These results therefore complement earlier work employing the same precursor and O_3 as the oxidant in an ALD process [33]. The ALD SiO_2 processes with this precursor are therefore of interest for high-volume manufacturing applications, for instance using ALD batch processes or inline (plasma) ALD equipment [34]. In a subsequent study, the interface properties of the SiO_2 films on Si will be evaluated in more detail by additional silicon surface passivation studies [35].

Acknowledgments

Dr. S.E. Potts is acknowledged for the fruitful discussions and B. Macco and Dr. M.A Verheijen for carrying out the AFM and TEM analysis, respectively. Ch. Lachaud, N. Blasco, and A. Madec from Air liquide are acknowledged for donating the SAM.24 precursor. This work is supported by Q-Cells, the German Ministry for the Environment, Nature Conservation and Nuclear Safety (BMU) under contract number 0325150 (“ALADIN”), and by the Dutch Technology Foundation STW (Thin Film Nanomanufacturing (TFN) program).

Downloaded 01 May 2011 to 131.155.217.116. Redistribution subject to ECS license or copyright; see http://www.ecsdl.org/terms_use.jsp

References

1. A. G. Aberle, *Prog. Photovoltaics* **8**, 473 (2000).
2. M. J. Kerr and A. Cuevas, *Semicond. Sci. Technol.* **17**, 35 (2002).
3. J. Zhao, A. Wang, M.A.Green, and F. Ferrazza, *Appl. Phys. Lett.* **73**, 1991 (1998).
4. O. Schultz, A. Mette, M. Hermle, and S. W. Glunz, *Prog. Photovolt: Res. Appl.* **16**, 317 (2008).
5. S.M. George, *Chem. Rev.* **110**, 111 (2010).
6. R. L. Puurunen, *J. Appl. Phys.* **97**, 121301 (2005).
7. J.W. Klaus, O.W. Ott, J.M.Johnson, S.M. George, *Appl. Phys. Lett.* **70**, 1092 (1997).
8. S.M. George, O. Sneh, A.C. Dillon, M.K. Wise, A.W. Ott, L.A. Okada, and J.D. Way, *Appl. Surf. Science* **82**, 460 (1994).
9. J. W. Klaus, O. Sneh, and S. M. George, *Science* **278**, 1934 (1997).
10. D. Hausmann, J. Becker, S. Wang, and R.G. Gordon, *Science* **298**, 402 (2002).
11. B. B. Burton, M. P. Boleslawski, A. T. Desombre, and S. M. George, *Chem. Mater.* **20**, 7031 (2008).
12. D. Hiller, R. Zierold, J. Bachmann, M. Alexe, Y. Yang, J. W. Gerlach, A. Stesmans, M. Jivanescu, U. Müller, J. Vogt, H. Hilmer, P. Löper, M. Künle, F. Munnik, K. Nielsch, and M. Zacharias, *J. Appl. Phys.* **107**, 064314 (2010).
13. S. Kamiyama, T. Miura, and Y. Nara, *Thin Solid Films* **515**, 1517 (2006).
14. S-J. Won, S. Suh, M. Soo Huh, and H. Joon Kim, *IEEE Electron Device Lett.* **31**, 857 (2010).
15. R. Katamreddy, B. Feist, and C. Takoudis, *J. Electrochem. Soc.* **155**, G163 (2008).
16. Burton, B.B., Rang, S.W., Rhee, S.W., and George, S.M., J. *Phys. Chem. C* **113**, 8249 (2009).
17. C. Dussarrat, WO Patent 2006/097525 (2006).
18. Air Liquide, 75 Quai d'Orsay, 75321, Paris Cedex 07, France, http://www.airliquide.com
19. J. L. van Hemmen, S. B. S. Heil, J. H. Klootwijk, F. Roozeboom, C. J. Hodson, M. C. M. van de Sanden, and W. M. M. Kessels, *J. Electrochem. Soc.* **154**, G165 (2007).
20. G. Dingemans, M.C.M. van de Sanden, W.M.M. Kessels, *Electrochem. Solid. State Lett.* **13**, H76 (2010).
21. G. Dingemans, R. Seguin, P. Engelhart, M. C. M. van de Sanden, and W. M. M. Kessels, *Phys. Status Solidi RRL* **4**, 10 (2010).
22. S.B.S. Heil, F. Roozeboom, M.C.M. van de Sanden, and W.M.M. Kessels, *J. Vac. Sci. Technol. A* **26**, 472 (2008).
23. S.E. Potts, W. Keuning, E. Langereis, G. Dingemans, M.C.M. van de Sanden, and W.M.M. Kessels, *J. Electrochem. Soc*. **157**, P66 (2010).
24. C. Dillon, A.W. Ott, J.D. Way, and S.M. George, *Surf. Sci.*, **322**, 230 (1995).
25. E. Langereis, J. Keijmel, M.C.M. van de Sanden, and W.M.M. Kessels, *Appl. Phys. Lett.* **92**, 231904 (2008).
26. B. Hoex, F.J.J. Peeters, M. Creatore, M.A. Blauw, W.M.M. Kessels, and M.C.M. van de Sanden, *J. Vac. Sci. Technol. A* 24, 1823 (2006).
27. S. B. S. Heil, J. L. van Hemmen, M. C. M. van de Sanden, and W. M. M. Kessels, *J. Appl. Phys.* 103, 103302 (2008).
28. A.J.M. Mackus, S.B.S. Heil, E. Langereis, H.C.M. Knoops, M.C.M. van de Sanden, and W.M.M. Kessels, *J. Vac. Sci. Technol. A* **28**, 77 (2010).
29. B. Hoex, S.B.S. Heil, E. Langereis, M.C.M. van de Sanden, and W.M.M. Kessels, *Appl. Phys. Lett.* **89**, 042112 (2006).

Downloaded 01 May 2011 to 131.155.217.116. Redistribution subject to ECS license or copyright; see http://www.ecsdl.org/terms_use.jsp

30. G. Dingemans, N. M. Terlinden, D. Pierreux, H. B. Profijt, M. C. M. van de Sanden, and W.M.M. Kessels, *Electrochem. Solid. State Lett.* **14**, H1 (2011).
31. N.E. Grant and K.R. McIntosh, *IEEE Electron Device Lett.* **31**, 1002 (2010).
32. G. Dingemans, M.C.M. van de Sanden, and W.M.M. Kessels, *Phys. Status Solidi RRL* (2011). DOI 10.1002/pssr.201004378
33. Air Liquide, Private communication.
34. G. Dingemans, N. M. Terlinden, D. Pierreux, H. B. Profijt, M. C. M. van de Sanden, and W. M. M. Kessels, *Electrochem. Solid-State Lett.* **14**, H1 (2011).
35. G. Dingemans, N.M. Terlinden, M.C.M. van de Sanden, and W.M.M. Kessels, to be published (2011)

Downloaded 01 May 2011 to 131.155.217.116. Redistribution subject to ECS license or copyright; see http://www.ecsdl.org/terms_use.jsp